ACS Catalysis

Letter

pubs.acs.org/acscatalysis

Tailoring Carbon Nanotube N-Dopants while Designing Metal-Free Electrocatalysts for the Oxygen Reduction Reaction in Alkaline Medium

Giulia Tuci,[†] Claudio Zafferoni,[‡] Primiano D'Ambrosio,[†] Stefano Caporali,[‡] Matteo Ceppatelli,[†,§] Andrea Rossin,[†] Theodoros Tsoufis,[†] Massimo Innocenti,*[,†,‡] and Giuliano Giambastiani*[,†]

[†]Institute of Chemistry of OrganoMetallic Compounds, ICCOM-CNR and INSTM Consortium, 50019 Sesto F.no, Florence, Italy

[‡]Department of Chemistry, University of Florence, 50019 Sesto F.no, Florence, Italy

[§]LENS − European Laboratory for Nonlinear Spectroscopy, 50019 Sesto F.no, Italy

Supporting Information

ABSTRACT: A straightforward, energy- and atom-saving process to the production of tailored N-doped and catalytically active metal-free carbon nanostructures, has been set up. Our ex situ approach to the N-decoration of the carbon nanotube sidewalls contributes to elucidate the complex structure−reactivity relationship of N-doped carbon nanomaterials in oxygen reduction reactions, providing fundamental insights on the nature of the N-active sites as well as on the role of neighboring carbons.

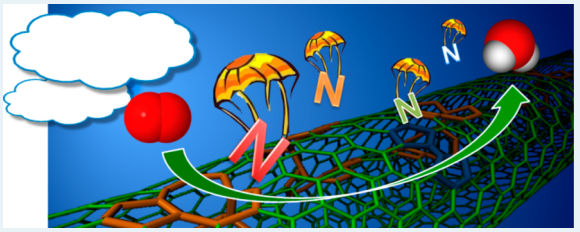

KEYWORDS: *ex situ N-doping, doped carbon nanotubes, aryl-diazonium salt chemistry, electrocatalysts, oxygen reduction reaction (ORR)*

Intensive research efforts have been devoted in the past few years to the development of efficient, durable, and inexpensive alternatives to precious-metal-based electrocatalysts (typically containing Pt and its alloys) for the oxygen reduction reaction (ORR) in fuel cell (FC) cathodes.[1] Typically, the ORR can proceed either through a four-electron process to combine oxygen with electrons and protons into water as the final product or through a less efficient two-step, two-electron pathway involving the formation of the hydroperoxide ions as intermediates.[1] On this basis, nitrogen-doped 1D and 2D carbon nanomaterials (occasionally combined with non-noble metal nanoparticles) have recently emerged as valuable candidates capable of promoting this reaction efficiently.[2] It is generally accepted that N-doped carbon nanostructures can favor the surface O_2 chemisorption/activation improving their catalytic performance in the ORRs remarkably.[2a,3]

Although a relatively high number of N-doped carbon nanostructures showing catalytic activity in ORRs have been prepared by the in situ CVD approach,[2] much less work has been done for the obtainment of catalytically active N-decorated carbon nanomaterials using milder and easily tunable ex situ (exohedral) organic functionalization techniques. The latter imply a number of important issues whose achievement may represent a real breakthrough in the development of novel nanostructured, metal-free catalysts. Indeed, in addition to leading to a fine-tuning of the chemical identity of the N-dopants, an ex situ approach better matches the requirements for energy- and atom-saving processes than the classical CVD approach. In addition, N-dopants are entirely present at the nanotube surface, where the catalytic process takes place. Finally, an ex situ approach can contribute to answering the widely debated question related to the intrinsic ability of different N-containing groups, randomly embedded in the sp^2 CNT network, at promoting ORRs.[4]

Although the real nature of the active sites in N-doped carbon nanomaterials still remains unclear, it is generally accepted that pyridine and pyrrole nitrogen atoms contribute differently to the ORR, the former playing a key role in promoting the process.[4] In this regard, a puzzling question arises: What is the effect of the neighboring atomic environment on the ability of pyridine nitrogen atoms to promote ORR? To answer this question, we took advantage of the well consolidated aryldiazonium salt (Tour) functionalization protocol[5] as a convenient synthetic methodology for the ex situ N-doping of MWCNTs with pyridine- and pyrrole-containing dangling groups (Scheme 1).

As shown in Scheme 1, 4-aminopyridine (**1**), 9-aminoacridine (**3**), and 3-aminocarbazole (**5**) are selected as N-containing candidates, **3** and **5** being selected as mimics of pyridine and pyrrole frameworks, respectively, embedded in a conjugated Csp^2 network. All reactions proceed smoothly under mild conditions, providing the expected functionalized samples **2**, **4**, and **6**. Careful workup procedures and parallel blank tests (carried out in the absence of the isopentylnitrite reagent) have been used to rule out any possible reagent

Received: May 22, 2013
Revised: July 17, 2013
Published: August 19, 2013

Scheme 1. CNTs Ex Situ Functionalization via Aryl Diazonium Salt (Tour) Conditions[a]

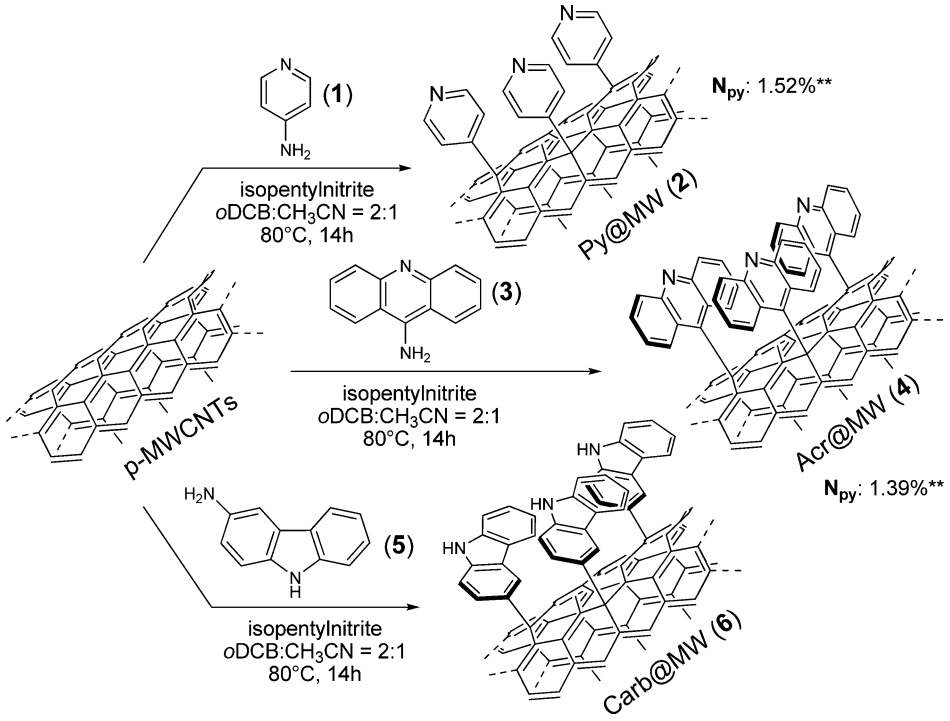

[a](**) The N_{py} content (N_{Py}%) is calculated for samples **2** and **4** via acid−base titration and reported as the average value over three independent runs (see the Supporting Information).

contamination resulting from simply physisorbed molecules (see the Supporting Information).

The as-synthesized N-doped materials have been spectroscopically (XPS, Raman) and morphologically (TEM) characterized. CHN elemental analysis on **2**, **4**, and **6** is used to calculate the functionalization loading (2.0 N at. % for **2**, 1.7 N at. % for **4**, and 2.8 N at. % for **6**), and an acid−base titration for the more basic samples **2** and **4** provides a well matching response on the pyridine group content (see the Supporting Information).[6] Finally, thermogravimetric analyses (TGA) give additional evidence of the occurred functionalization process (Supporting Information Figure S1). More gradual decomposition profiles observed for all N-doped samples are indicative of a substantial sidewall perturbation as consequence of the functionalization procedure. XPS spectra of the N-containing samples present characteristic N 1s profiles. Peaks at 398.6 eV for **2** and **4**, and 400.2 eV for **6** (Supporting Information Figure S2) are attributed to pyridinic nitrogen[7] and pyrrole-type-containing groups, respectively. Minor components at higher binding energy values arise from the N 1s spectra of both pyridine containing samples and are ascribed to commonly observed surface contaminations.[5e,g,7] Raman spectra of all the N-decorated materials (Supporting Information Figure S3) do not show any significant change in the I_D/I_G values as compared with the pristine sample, thus revealing only negligible crystallite and defect site surface density alterations. Similarly, TEM images of the N-decorated samples do not reveal any significant morphological difference in terms of tube length and diameter compared to the pristine one; slightly deaggregated tube bundles appear for the functionalized samples throughout the whole scanned area (Supporting Information Figure S4).

The as-prepared N-decorated CNT samples have been scrutinized with respect to their catalytic performance in ORRs.[2] To evaluate their electrocatalytic activity, N-CNTs/Nafion films deposited on a rotating glassy carbon (GC) electrode have been preliminarily investigated by cyclic voltammetry (CV) using a three-electrode cell operating in O_2-saturated 0.1 M KOH solution. Under O_2-saturated conditions, the N-decorated samples show an irreversible ORR peak not present under N_2-saturated electrolyte conditions (Figure 1).

To gain further insights on the ORR electrochemical performance of the ex situ N-doped samples, rotating ring disk electrode (RRDE) voltammograms have been systemati-

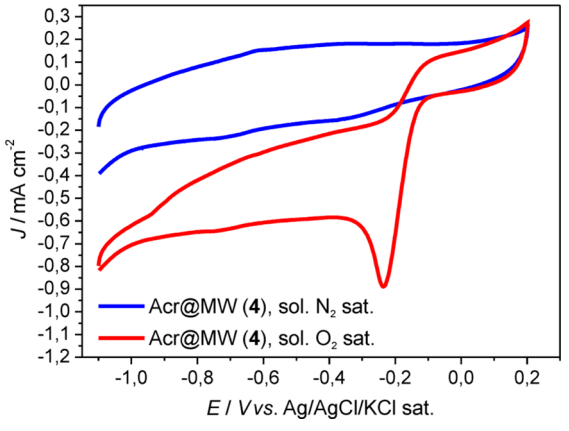

Figure 1. Cyclic voltammograms for sample Acr@MW (**4**) in N_2-saturated (blue) and O_2-saturated solutions (red). The potential was linearly swept from −1.1 to 0.2 V at a scan rate of 5 mV s^{-1}. Ag/AgCl/KCl sat. was employed as the reference electrode.

dx.doi.org/10.1021/cs400379h | ACS Catal. 2013, 3, 2108−2111

cally acquired (Supporting Information Figure S5). The amount of the N-decorated material deposited on the RRDE is maintained constant and fixed to the optimal value measured on sample **4** (see the Supporting Information, electrochemical data processing).

Figure 2 illustrates the ORR polarization curves of the three N-doped samples (**2**, **4**, **6**), compared with pristine MWCNTs,

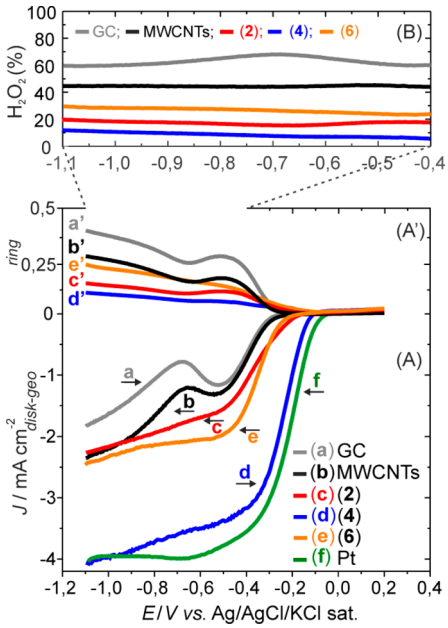

Figure 2. (A) Current–potential curves at 293 K for ORR in O_2 saturated 0.1 M KOH solution for the disk electrode [0.196 cm^2 GC rotating-disk electrode] and (A′) for the ring electrode [0.11 cm^2 Pt rotating-ring electrode]. All samples are measured at an angular rotation rate (f) of 800 rpm. (B) H_2O_2 production (%) for all N-doped and undoped samples (see also the Supporting Information).

GC, and Pt-based electrocatalysts, along with the respective H_2O_2 production.[8] For all ORR profiles reported in Figure 2, background currents, measured under saturated N_2 conditions, are subtracted from the respective curves to eliminate all capacitive contributions.

Linear-sweep voltammograms (LSVs) for each sample at different spin rates are shown in Supporting Information Figure S5. Potentials are linearly swept from −1.1 to 0.2 V and finally reversed against an Ag/AgCl/KCl sat. as reference electrode at a scan rate of 5 mV s^{-1}. As Figure 2 shows, the onset potentials (E_{on}) of all C-based catalysts are negatively shifted from the E_{on} value measured for the Pt electrocatalyst. It is noteworthy that although ORR starts at −0.181 V (E_{on}) on **2**, corresponding to an overpotential of ∼80 mV compared with Pt, less than 40 mV (overpotential) is measured for **4**. Compared with pristine CNTs and samples **2** and **6**, the ORR onset potential measured for **4** is shifted to a more positive value featuring a remarkably higher electrocatalytic activity (Figure 2 and the Supporting Information Figure S5). The average number of electrons ($n_{E=-1V}$) transferred for O_2 molecule in the ORR process is calculated according to the Koutecky–Levich (K–L) equation, and relative values are outlined in Table 1.[9,10]

The K–L plots (J^{-1} vs $f^{-1/2}$) of each catalyst, obtained from LSVs according to J values measured at −1 V, show good linearity at various rotation speeds (Figure 3), implying a first-order reaction toward dissolved O_2.

Table 1. E_{on} Values (V), Average Number of Electrons Transferred ($n_{E=-1\ V}$) for O_2 Molecule and Average Yield of Peroxide Formation in 0.1 KOH[a]

catalyst	E_{on} (V)	$n_{E=-1V}$	H_2O_2 (%)[b]
GC	−0.307	2.0	64
MWCNTs	−0.299	2.5	48
Py@MW (**2**)	−0.181	2.9	24
Acr@MW (**4**)	−0.139	3.2	10
Carb@MW (**6**)	−0.250	2.5	32
Pt	−0.101	4.1	

[a]Data derived from Figures 2 and 3. [b]Average values calculated in the −0.4 ÷ −1 E/V range.

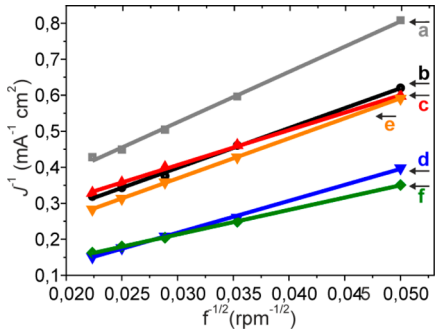

Figure 3. K–L plots for **2**, **4**, **6**, GC, MWCNTs, and Pt catalysts as obtained from the respective LSVs.[9] Parameters used: O_2 concentration (C), 1.15 × 10^{-3} mol L^{-1}; O_2 diffusion coefficient (D), 1.95 × 10^{-5} cm^2 s^{-1}; kinematic viscosity (ν) of the electrolyte solution, 0.008977 cm^2 s^{-1} (see the Supporting Information).

The calculated n value for the ORR catalyzed by **4**, as measured at high overpotential (E = −1 V), suggests a largely prevailing four-electron process. This is further confirmed by the moderate ring current recorded for this catalyst at the Pt rotating ring-disk electrode along with the modest percentage of H_2O_2 produced (Figure 2 and the Supporting Information).[10]

As can be inferred from these data, pyridinic nitrogen sites are responsible in part for the final catalyst performance, whereas neighboring carbon atoms seem to play an essential role in the catalyst's ability to perform ORR efficiently.[4] Indeed, pyridine units embedded in a conjugated (although spatially limited) sp^2 carbon network dramatically improve the catalyst performance both in terms of E_{on} and diffusion-limited current density values (J) (Table 1, catalyst **4** vs **2** and Figure 2). Such a result helps to shed light on the complex structure–reactivity relationship of N-doped carbon nanomaterials with respect to their catalytic performance in ORRs. Furthermore, electron-accepting nitrogens are known to impart a relatively high positive charge density on the adjacent carbon atoms; the resulting N–C_α bond polarization is expected to weaken the O–O bond, thus facilitating the ultimate O_2 reduction path. DFT calculations of Mulliken atomic charges at the B3LYP//6-31G** level of theory show an increment of the N–C_α bond polarization while moving from simple pyridine to acridine frameworks ($[|q_N| + |q_{C\alpha}|]_{Py}$ = 0.50e; $[|q_N| + |q_{C\alpha}|]_{Acr}$ = 0.65e; Supporting Information Table S3).[2a] All these data taken together strongly support the hypothesis of a truly operative *side-on* O_2 adsorption mode (Yeager model) with respect to a classical *end-on* one (Pauling model) (Figure 4).[2a,4b]

dx.doi.org/10.1021/cs400379h | ACS Catal. 2013, 3, 2108–2111

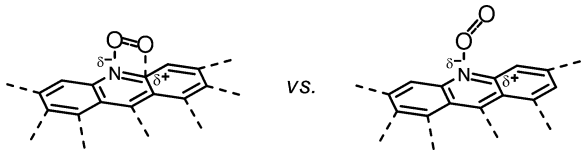

Figure 4. Yeager model (side-on) vs Pauling model (end-on).

In line with literature precedents for variably N-doped in situ prepared carbon nanomaterials containing relatively high N-pyrrolic fractions,[4,11] our carbazole-based system **6** shows only moderate electrocatalytic performance, together with a relatively high H_2O_2 production (Figures 2 and 3). In addition, the catalytic activity gap measured between **4** and **6** is even more remarkable while considering the higher surface N-loading on **6** as it results from the experimental data (>50% based on N-elemental analysis; see the Supporting Information).

In summary, a straightforward single step and reproducible approach to the production of tailored N-doped and catalytically active carbon nanostructures, has been set up. Compared with the classical in situ approach, our ex situ method, in addition to providing fundamental insights on the complex structure−reactivity relationship of N-doped carbon nanomaterials in ORRs, lists a number of remarkable advantages: (1) mild reaction conditions required to N-decorate the CNTs surface (energy-saving process); (2) easy tailoring of the N-containing functional groups and (3) their full exposure (atom-saving) to the nanomaterial outer side, where the catalytic process takes place; and (4) absolutely remarkable electrocatalytic activity and long-term stability of selected N-doped metal-free samples for ORRs in basic medium. As for the latter point, ink of catalyst **4** presents a complete reproducibility of its electrochemical performance in successive CV cycles while maintaining its electrochemical properties almost unchanged when simply stored at room temperature for months. Owing to the established versatility of the Tour functionalization protocol with both 1D and 2D nanomaterials,[12] the methodology developed in this study can be conveniently applied to the ex situ heterodecoration of different nanocarbon materials with light elements for the production of metal-free catalysts.

■ ASSOCIATED CONTENT

Supporting Information

Synthesis, characterization, and catalytic details on electrochemical tests for **2**, **4** and **6**. This material is available free of charge via the Internet at http://pubs.acs.org.

■ AUTHOR INFORMATION

Corresponding Author

*Phone: +39 055 5225288. Fax: +39 055 5225203. E-mail: giuliano.giambastiani@iccom.cnr.it.

Notes

The authors declare no competing financial interest.

■ ACKNOWLEDGMENTS

The authors thank the *FreeCats* project (NMP3-SL-2012-280658) for financial support to this work.

■ REFERENCES

(1) (a) Minhua, S. In *Electrocatalysis in Fuel Cells, A Non- and Low-Platinum Approach*; Minhua, S., Ed.; Springer: London; 2013; p 327. (b) Su, D. S.; Zhang, J. Z.; Frank, B.; Thomas, A.; Wang, X.; Paraknowitsch, J.; Schlögl, R. *ChemSusChem* **2010**, *3*, 169−180. (c) Markovic, N. M.; Schmidt, T. J.; Stamenkovic, V.; Ross, P. N. *Fuel Cells* **2001**, *1*, 105−116. (d) Chen, Z.; Higgins, D.; Yu, A.; Zhang, L.; Zhang, J. *Energy Environ. Sci.* **2011**, *4*, 3167−3192. (e) Chisaka, M.; Suzuki, Y.; Iijima, T.; Sakurai, Y. *J. Phys. Chem. C* **2011**, *115*, 20610−20617.

(2) (a) Gong, K.; Du, F.; Xia, Z.; Durstock, M.; Dai, L. *Science* **2009**, *323*, 760−764. (b) Chizari, K.; Deneuve, A.; Ersen, O.; Florea, I.; Liu, Y.; Edouard, D.; Janowska, I.; Begin, D.; Pham-Huu, C. *ChemSusChem* **2012**, *5*, 102−108. (c) Morozan, A.; Jégou, P.; Pinault, M.; Campidelli, S.; Jousselme, B.; Palacin, S. *ChemSusChem* **2012**, *5*, 647−651. (d) Li, Y.; Zhou, W.; Wang, H.; Xie, L.; Liang, Y.; Wei, F.; Idrobo, J.-C.; Pennycook, S. J.; Dai, H. *Nat. Nanotechnol.* **2012**, *7*, 394−400. (e) Geng, D.; Chen, Y.; Chen, Y.; Li, Y.; Li, R.; Sun, X.; Ye, S.; Knights, S. *Energy Environ. Sci.* **2011**, *4*, 760−764. (f) Parvez, K.; Yang, S.; Hernandez, Y.; Winter, A.; Turchanin, A.; Feng, X.; Müllen, K. *ACS Nano* **2012**, *6*, 9541−9550. (g) Yu, D.; Nagelli, E.; Du, F.; Dai, L. *J. Phys. Chem. Lett.* **2010**, *1*, 2165−2173. (h) Unni, S. M.; Devulapally, S.; Karjule, N.; Kurungot, S. *J. Mater. Chem.* **2012**, *22*, 23506−23513. (i) Qu, L.; Liu, Y.; Baek, J.-B.; Dai, L. *ACS Nano* **2010**, *4*, 1321−1326. (l) Rao, C. V.; Ishikawa, Y. *J. Phys. Chem. C* **2012**, *116*, 4340−4346.

(3) (a) An, W.; Turner, C. H. *J. Phys. Chem. C* **2009**, *113*, 7069−7078. (b) Kaukonen, M.; Krasheninnikov, A. V.; Kauppinen, E.; Nieminen, R. M. *ACS Catal.* **2013**, *3*, 159−165. (c) Kim, H.; Lee, K.; Woo, S. I.; Jung, Y. *Phys. Chem. Chem. Phys.* **2011**, *13*, 17505−17510.

(4) (a) Kuroki, S.; Nabae, Y.; Chokai, M.; Kakimoto, M.-a.; Miyata, S. *Carbon* **2012**, *50*, 153−162. (b) Feng, L.; Yan, Y.; Chen, Y.; Wang, L. *Energy Environ. Sci.* **2011**, *4*, 1892−1899. (c) Rao, C. V.; Cabrera, C. R.; Ishikawa, Y. *J. Phys. Chem. Lett.* **2010**, *1*, 2622−2627.

(5) (a) Bahr, J. L.; Tour, J. M. *Chem. Mater.* **2001**, *13*, 3823−3824. (b) Dyke, C. A.; Tour, J. M. *J. Am. Chem. Soc.* **2003**, *125*, 1156−1157. (c) Dyke, C. A.; Tour, J. M. *Nano Lett.* **2003**, *3*, 1215−1218. (d) Hudson, J. L.; Casavant, M. J.; Tour, J. M. *J. Am. Chem. Soc.* **2004**, *126*, 11158−11159. (e) Dyke, C. A.; Stewart, M. P.; Maya, F.; Tour, J. M. *Synlett* **2004**, *1*, 155−160. (f) Price, B. K.; Hudson, J. L.; Tour, J. M. *J. Am. Chem. Soc.* **2005**, *127*, 14867−14870. (g) Price, B. K.; Tour, J. M. *J. Am. Chem. Soc.* **2006**, *128*, 12899−12904. (h) Doyle, C. D.; Tour, J. M. *Carbon* **2009**, *47*, 3215−3218.

(6) For related titration procedures, see: (a) Ballesteros, B.; de la Torre, G.; Ehli, C.; Aminur Rahman, G. M.; Agulló-Rueda, F.; Guldi, D. M.; Torres, T. *J. Am. Chem. Soc.* **2007**, *129*, 5061−5068. (b) Moaseri, E.; Baniadam, M.; Maghrebi, M.; Karimi, M. *Chem. Phys. Lett.* **2013**, *555*, 164−167.

(7) Daletoua, M. K.; Paloukisa, F.; Stefopoulosa, A. *ECS Trans.* **2009**, *25*, 1915−1924.

(8) Neergat, M.; Gunasekar, V.; Rahul, R. *J. Electroanal. Chem.* **2011**, *658*, 25−32.

(9) Bard, A. J.; Faulkner, L. R. In *Electrochemical Methods: Fundamentals and Applications*, 2nd ed.; John Wiley & Sons, Inc.: New York, 2001, pp 856.

(10) Wang, Y.; Zhang, D.; Liu, H. *J. Power Sources* **2010**, *195*, 3135−3139.

(11) (a) Yu, D.; Zhang, Q.; Dai, L. *J. Am. Chem. Soc.* **2010**, *132*, 15127−15129. (b) Shanmugam, S.; Osaka, T. *Chem. Commun.* **2011**, *47*, 4463−4465. (c) Kundu, S.; Nagaiah, T. C.; Xia, W.; Wang, Y.; Van Dommele, S.; Bitter, J. H.; Santa, M.; Grundmeier, G.; Bron, M.; Schuhmann, W.; Muhler, M. *J. Phys. Chem. C.* **2009**, *113*, 14302−14310.

(12) (a) Kuila, T.; Bose, S.; Mishra, A. K.; Khanra, P.; Kim, N. H.; Lee, J. H. *Prog. Mater. Sci.* **2012**, *57*, 1061−1105. (b) Liu, J.; Tang, J.; Gooding, J. J. *J. Mater. Chem.* **2012**, *22*, 12435−12452.